SEDIMENTATION OF A NON-SPHERICAL SOLID PARTICLE UNDER INFLUENCES OF FLOW DISTURBANCES

YASUO HATTORI
Central Research Institute of Electric Power Industry, Abiko, Japan, yhattori@criepi.denken.or.jp

HITOSHI SUTO
Central Research Institute of Electric Power Industry, Abiko, Japan, suto@criepi.denken.or.jp

KEISUKE NAKAO
Central Research Institute of Electric Power Industry, Abiko, Japan, nakao@criepi.denken.or.jp

KIYOSHI TOSHIDA
Central Research Institute of Electric Power Industry, Abiko, Japan, toshida@criepi.denken.or.jp

MITSUHARU NOMURA
Central Research Institute of Electric Power Industry, Abiko, Japan, nomuharu@criepi.denken.or.jp

ABSTRACT

We experimentally investigated dynamics of sand-silica particles in an upward air field, which mimics sedimentation of the particles in a river flow, especially paying attention to interactions between the dynamics and fluctuating velocities (turbulences) accompanied with the upward flow. The velocity of upward flow was set to the terminal velocities of the particles in air flows. A vertical wind-tunnel with an active grid was used to generate upward flows with turbulences. Size, shape and movement of particles seeded in a test section were measured by a shadowgraph technique; the particles were illuminated by high-intensity pulsed lasers, Nd: YAG laser, with an optical diffuser, and were captured by a CCD camera with a long-distance microscope lens, which was placed in front of the light source. After confirming that the experimental set-up has a capability to capture the movement and shape of particles, i.e., measured settling velocities without upward flows agree well with terminal velocities estimated by empirical formula proposed in previous studies, we revealed that the typical characteristics for dynamics of non-spherical particles in the upward flows with turbulences. The particles mainly choose two orientations, vertical and horizontal orientations in the flow, causing the scatter of terminal velocities. Also, the turbulences in the upward flows drastically decrease the terminal velocities with changes in the orientation of particles.

Keywords: Deposition, Lab test, Shadow imaging technique, Terminal velocity, Turbulence

1. INTRODUCTION

The details of settling behavior of a non-spherical particles are still unknown, while a better understanding of dynamics of a non-spherical particle in a flow field with disturbances (turbulences) is of practical interest in civil engineering, including river engineering. Indeed, many empirical formulas for the terminal velocities, which is one of the most important thermal property for engineering applications, have been already reported, but there exists considerable scattering of calculations among them even under an ideal condition, such as in the flow fields without turbulence (Folch 2012). The lack of an understanding of dynamics of a non-spherical particle might be due to extreme difficulty in executing experiments. The experiments have a formidable hurdle on measurements of movements with size and shape of a particle simultaneously.

In the present study, we carried out wind tunnel experiment (lab test) by using a shadowgraph technique with high-intensity pulsed laser and long-distance microscope lens to examine dynamics of a non-spherical particle, especially paying attention to effects of turbulence including flow fields. Sand-silica particles are seeded in a test section of a vertical wind-tunnel with an active grid, which generates upward air flows with turbulence, and shape, size and movements of particles in flow fields, which mimics sedimentation of the particles in a river flow, were measured. After confirming the accuracies of measurements, the typical characteristics for dynamics of non-spherical particles in the upward flows with turbulences are discussed in details.

2. EXPERIMENTAL SETUP

We used the same wind-tunnel experimental technique of our previous study (Hattori et al., 2010; Hattori et al. 2018). The experiment was conducted in a vertical wind tunnel at the Central Research Institute of Electric

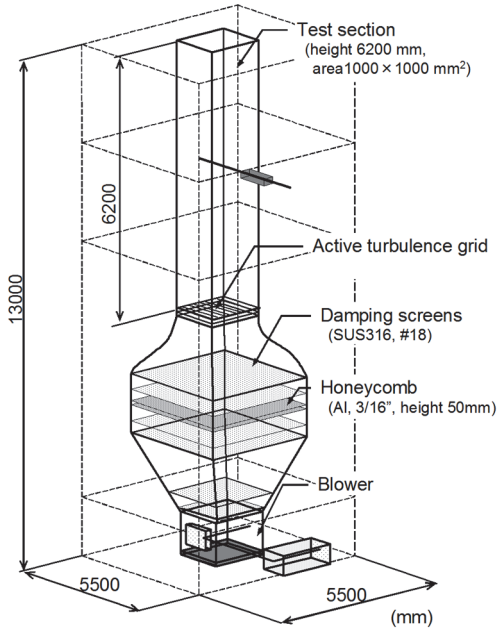

Figure 1. Schematic of vertical wind tunnel

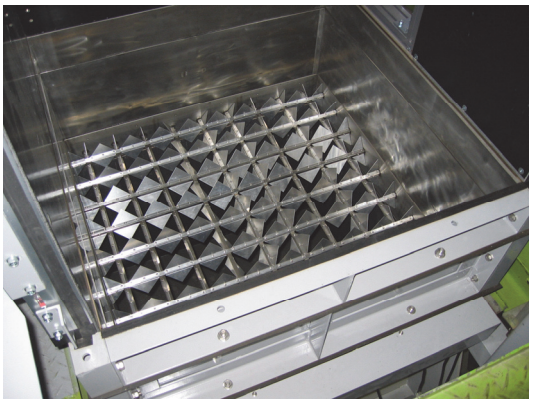

Figure 2. Photograph of active turbulence grid in test section of wind tunnel; the side walls were removed to take picture.

Power Industry, as shown in Fig. 1 (Hattori et al., 2000; Hattori et al. 2001). The test section settled vertically was 1000×1000 mm^2 in area and 6200 mm long, and the walls of the test section are made of smooth flat wood plates. The active grid, which was devised by Makita et al. (1987) and has been widely used research on isotropic turbulences of high Reynolds number (e.g. Mydlarski and Warhaft 1996; Porte and Biesheuvel 2002; Kang et al. 2003; Savelsberg and Water 2008), was used to control the turbulence characteristics of upward flows. Figure 2 presents the photograph of our active grid, which was installed at the front of the test section. The design followed those of previous studies, composing of rotating grid bars with attached triangular agitator wings, stepping motors located at the end of each grid bards outside the wind tunnel and a controller. The mesh spacing L_M between the grid bars was 110 mm. Each of the 18 grid bars with wings independently flapped with a stepping motor controlled by a program on PC.

The samples of measurements were silica sands no.8, the grain size and the density of which are 50 – 200 μm and 2300 kg m^{-3} in the specification, respectively. These silica sands were seeded at the center of the test section. The velocity of upward flow at the centerline of the test section was set at 0.8 m s^{-1} to control the terminal velocities of sand silica particles in the air, which correspond to those in the water (river). We performed two experiments: one has no disturbance with all grid bars of the active grid remain at rest, and the other has a disturbance with each of the active grid bars flaps in a random way. For the latter case, the flapping angles of the grid bars were randomly varied in time, with the maximum angle at 60°. The mean rotation speed was set to 2 r.p.s. The measuring location, which was fixed at the downstream distance from the active turbulence grid of 4180 mm (= $38L_M$).

Figure 3 displays the normalized power spectra, $fE_{11}(f)/\sigma(u)^2$ and $fE_{33}(f)/\sigma(w)^2$, against frequency f of upward flows at the measuring location, where $\sigma(u)$ and $\sigma(w)$ are standard deviations of streamwise- and spanwise-velocity fluctuations, u and w, respectively. The velocity fluctuations were measured by an x-type hot wire anemometer (Hattori et al., 2010). The comparison of their peak frequencies shows that the length scale of u is

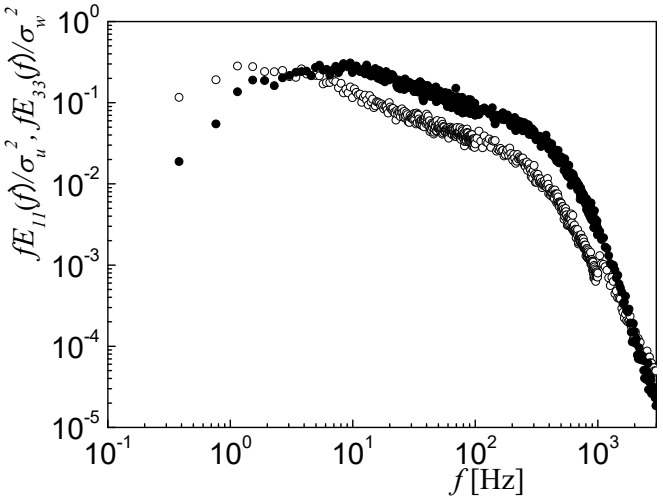

Figure 3. Power spectra of streamwise (vertical)- and horizontal-velocity fluctuations u and w in upward flow at measuring location (at x/L_M =38 and center of test section). Open- and closed-circles are for u and w.

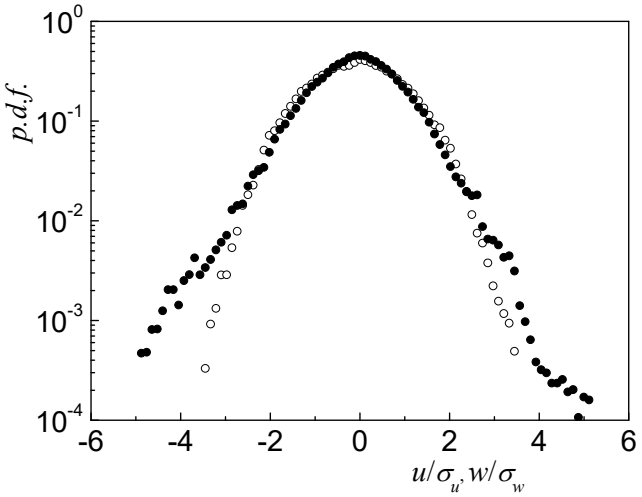

Figure 4. Probability density function of streamwise (vertical)- and horizontal-velocity fluctuations u and w in upward flow at measuring location (at x/L_M =38 and center of test section). Open- and closed-circles are for u and w, respectively.

much longer than that of w, implying that the large-scale disturbance eddy structure is elongated in the streamwise direction. The probability density functions of streamwise- and spanwise-velocity fluctuations are shown in Fig. 4. They are approximately Gaussian, the skewness and flatness factors of u are S(u) = 0.07 and F(u) = 2.95, and those factors of w are S(w) = 0.08 and F(w) = 3.48. These values agree well with other experiments that used an active grid (e.g. Mydlarsi and Warhaft 1996).

The size, shape and movement of particles seeded in the test section were measured by using a shadowgraph technique with high-intensity pulsed lasers and long-distance microscope lens to ensure spatio- and temporal resolutions for capturing moving particles. The shadow image instruments, which were located outside the test section for preventing disturbances on upward flows, comprised a particle feeder, light source and optics, CCD camera, synchronizer, and PC. The particles were added to the flow field in the test section by using the particle feeder. The distance between the lens and the object plane was set to 800 mm, giving the physical size of measuring area was 90 × 90 mm^2 and the spatial resolution of the image was 0.04 mm. The flow fields including particles were illuminated by laser lights formed with a double pulse YAG laser, the output and wavelength of which are 90 mJ/pulse and 532 nm, and the diffuser lens. The time interval between the two pulsed illuminations was set at 1.0 ms to keep the maximum displacement of successive particle images below the half of the visualized area approximately. The shadow images of particles in the illuminated flow fields were captured by a CCD camera (2048 × 2048 pixels) with the attachment of a long-distance microscope lens; the capture timing was controlled by the PC and synchronizer and the sampling frequency were set at 16Hz. The visualized images captured by the camera were stored temporally into a memory of camera and then into a PC hard disk. The duration of each image sequence was 4s. The restriction of data transfer rate did not permit small intervals between the sequences. Thus, we repeated the experiments under the same conditions and setup, and obtained

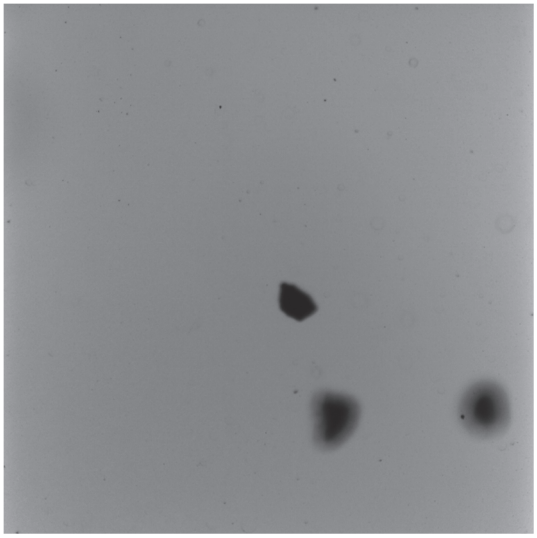

Figure 5. Example of visualized image.

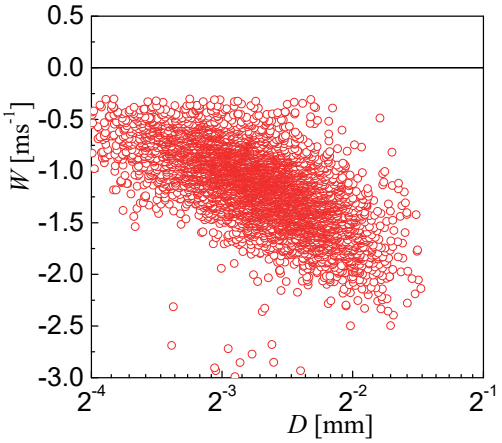

Figure 6. measured terminal velocities against the equivalent diameter under flow conditions without upward flow.

many visualized images, which is larger than 400s. Size, shape and movement of particles were calculated with the stored images.

Figure 5 depicts an example of image in whole visualized area. The flow direction is upward (from the bottom to the top) in the figure. This example clearly shows that the diffused laser light provides the background luminance with the same gray level, which is suit for generating shadow images of particles, and also the long-distance microscope lens gives thin depth of field. Namely, there exist shadow-images of particles with steep and gentle gradients at the edge (deep and shallow depth of gray level). Then, we calculated size, shape and movement of particles by using only the shadow images with steep gradient and deep depth of gray level to ensure the accuracies of statistics.

3. RESULTS

Firstly, we performed demonstrate measurements to verify the accuracy of measurement in the preliminary experiment without upward flows to compared with the terminal velocities of particles. Figure 6 presents measured velocities of horizontal and vertical components, U and W, against the particle size (measured equivalent diameter, D). Here, the negative and positive vertical velocities correspond to the upward and downward motions of particles, respectively. The horizontal velocities, W, are almost zero regardless to D, indicating that movements in the vertical direction is much dominant compared with those in the horizontal direction. The absolute values of vertical velocities, W, increases with the equivalent diameter, D. The increase rate of the absolute values changes at $D \cong 2^{-3}$ mm. These profiles of vertical velocities with equivalent diameters correspond to those of empirical formulas (Folch 2012)

Figure 7 shows the probability density functions, p.d.f.s, of equivalent diameter, D. The profiles of p.d.f.s, which is naturally independent of the flow conditions, generate the wide range of particle size from 2^{-4} to 2^{-1} mm, and also skew from that of Gaussian. The peak of profiles appears at $D \cong 125\mu$m ($=2^{-3}$ mm), corresponding to the value in the specification of silica sands no.8.

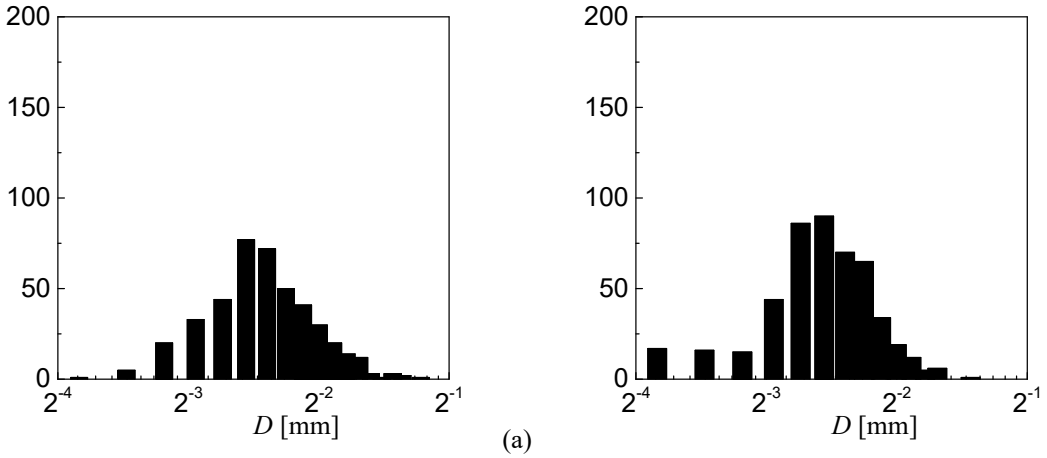

Figure 7. P.d.f of equivalent diameter, D, of particles, without turbulence (a), and with turbulence (b).

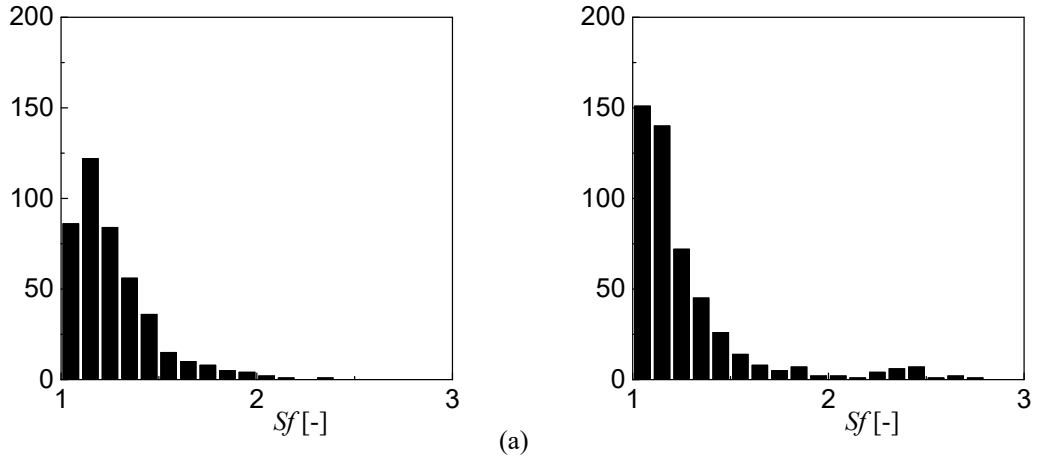

Figure 8. P.d.f of shape factor, Sf, of particles, without turbulence (a), and with turbulence (b).

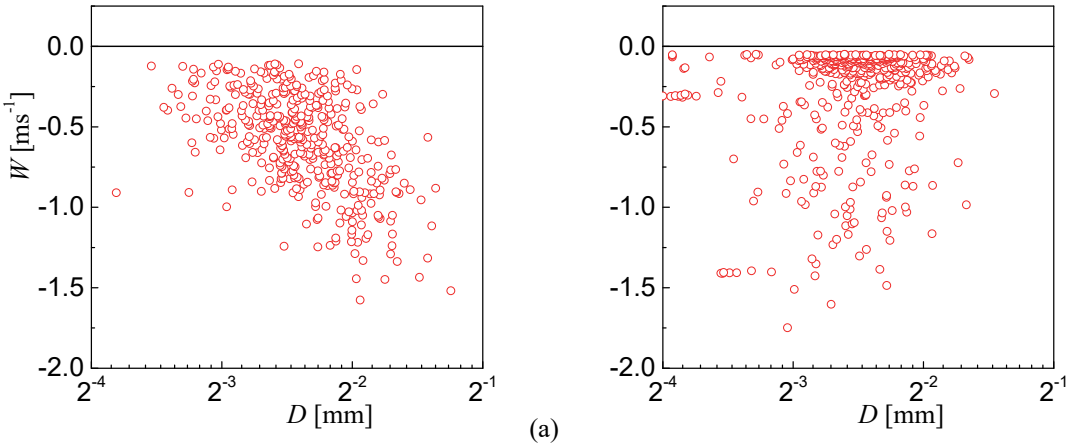

Figure 9. Relationship between terminal velocity and equivalent diameter of particles without turbulence (a), and with turbulence (b).

Figure 8 shows the p.d.f.s of the shape factor, Sf, which is defined by the circularity, $Sf = P^2/(4\pi S)$, where P and S are the perimeter and the area of the shadow image of a particle, respectively. These profiles are, also, naturally independent of the flow conditions, while turbulences in flow fields seem to provide the tendency of bipolarization, i.e., the particles with $Sf \cong 1$ and 3 increase with the addition of the turbulences in upward flows. Some particles take the large values of shape factor, $Sf > 2$, indicating that the present measurement firmly capture the data of non-spherical particles.

Figure 9 shows the relationship between vertical velocities, W, and the equivalent diameter, D. Here, the negative vertical velocities correspond to the downward motions of particles, also shown in Fig. 6. All particles takes negative values of W, indicating the descended particles in the test section. The settling velocities

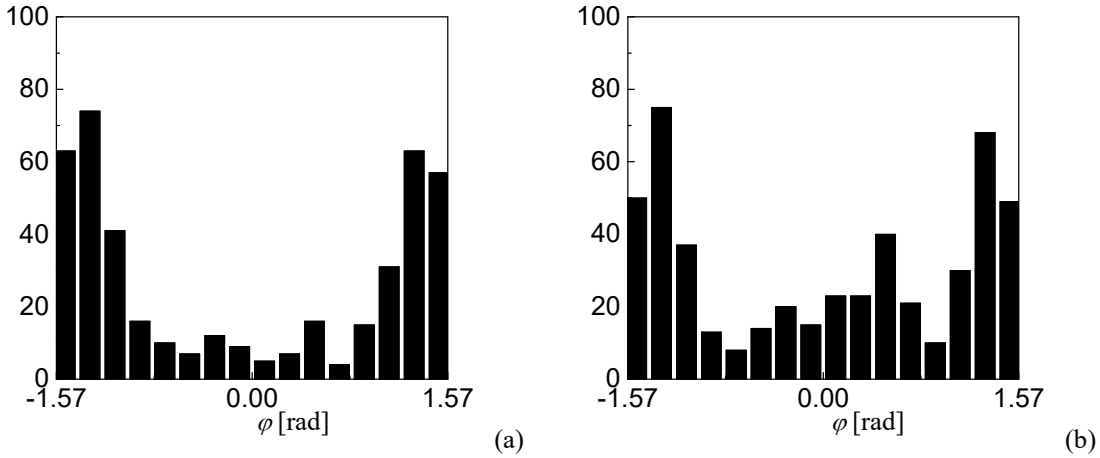

Figure 10. P.d.f. of orientation of particles without turbulence (a), and with turbulence (b).

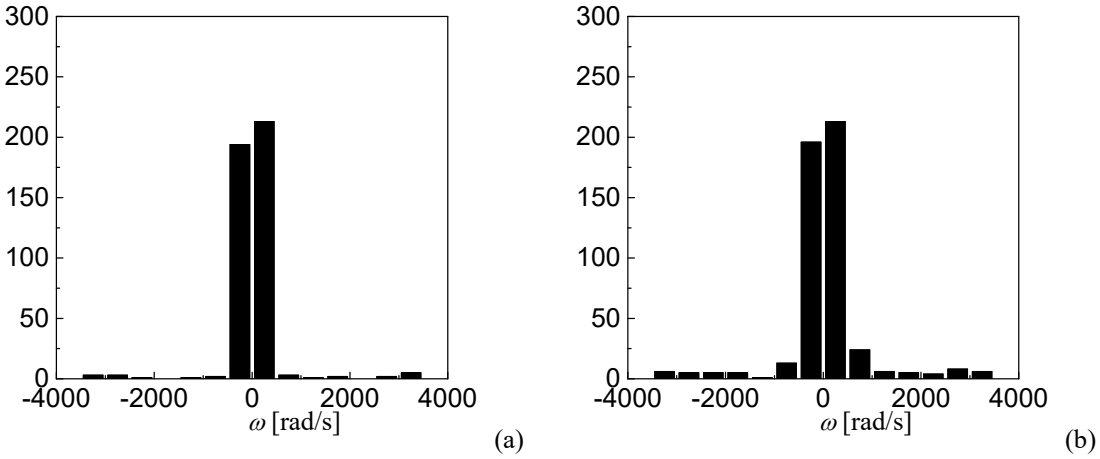

Figure 11. P.d.f. of angular velocity of particles without turbulence (a), and with turbulence (b).

significantly decrease due to the turbulences in upward flows. For instance, the velocities of $D \cong 2^{-2}$ mm are about 1ms^{-1} without turbulences whereas those mainly less than 0.5 ms^{-1} with turbulences.

Figure. 10 shows the p.d.f.s of orientations of particles, ϕ, against the equivalent diameter, D. Here, the definition of the orientation gives $\phi = 0$ and $\pm\pi/2$ for the particles with the horizontal and vertical main axis, respectively. The main axis of non-spherical particles apparently has a tendency to be vertically ($\phi \cong \pm\pi/2$), which might decrease the aerodynamic force for the particles. As to the effects of turbulences in the upward flow, we found that the additions in turbulences to the upward flow weaken the tendency, i.e., particles with the horizontal main axis ($\phi \cong 0$) increase.

Figure 11 shows the p.d.f.s of angular velocities, ω, against the equivalent diameter, D. The comparison of profiles indicates that the turbulences in the upward flows provide the increases in the absolute values of angular velocities.

4. SUMMARY AND DISCUSSION

We experimentally investigated dynamics of sand-silica no.8 in an upward air field, which mimics sedimentation of the particles in a river flow, especially paying attention to interactions between the dynamics and fluctuating velocities (turbulences) including the upward flow. A vertical wind-tunnel with an active grid was used to generate upward flows with turbulences. These silica sands were seeded at the center of the test section. The velocity of upward flow at the centerline of the test section was set at 0.8 m s^{-1} to control the terminal velocities of sand silica particles in the air, which correspond to those in the water (river). Size, shape and movement of particles seeded in a test section were measured by a shadowgraph technique. Firstly, we confirmed that the experimental set-up has a capability to capture the movement and shape of particles, i.e., measured settling velocities without upward flows increases with the diameter of particle, corresponding to the Stokes law. Also, we suggested that the scatter of measured settling velocities might be due to the variation of the orientation of particles in the air, which gives the change in the drag forces to particles. As to the effects of turbulences in the flow fields on dynamics of non-spherical particles, we revealed that the particles mainly

choose two orientations, vertical and horizontal orientations in the flow and the turbulences in flows drastically decrease the terminal velocities with changes in the orientation of particles.

ACKNOWLEDGMENTS

The authors wish to express our gratitude to Mr. Y. Futawatari of Dantec Dynamics, Ltd. for helpful comments on the design of the optical setup and to Dr. S. Takeuchi for fruitful discussion on this study.

REFERENCES

Folch A (2012) A review of tephra transport and dispersal models: evolution, current status, and future perspectives. J Volcanology and Geothermal Research 235-236:96-115.

Hattori Y, Tsuji T, Nagano Y, Tanaka N (2000) Characteristics of turbulent combined-convection boundary layer along a vertical heated plate. Int J Heat Fluid Flow 21: 520-525.

Hattori Y (2001) Turbulent characteristics and transition behavior of combined-convection boundary layer along a vertical heated plate, ph.D thesis, Nagoya Institute of Technology.

Hattori Y, Moeng C-H, Suto H, Tanaka N, Hirakuchi H (2010) Wind-tunnel experiment on logarithmic-layer turbulence under the influence of overlying detached eddies. Boundary-Layer Meteorol 134:269-283.

Hattori Y, Suto H, Nakao K, Hirakuchi H (2018) insight into coherence structure in logarithmic region of wall turbulence with detached eddy by using conditionally averaged two-camera PIV measurements. J Flow Visualization and Image Processing 25:1-14.

Kang HS, Chester S, Meneveau C (2003) Decaying turbulence in an active-grid- generated flow and comparisons with large-eddy simulation. J Fluid Mech 480: 129-160.

Mydlarski L, Warhaft Z (1996) On the onset of high-Reynolds-number grid-generated wind tunnel turbulence. J Fluid Mech 320: 331-368.

Poorte REG, Biesheuvel A (2002) Experiments on the motion of gas bubbles in turbulence generated by an active grid. J Fluid Mech 461: 127-154.

Savelsberg R, Water W (2008) Turbulence of a free surface. Phy review lett. Doi: 10.1103/PhysRevlett.100.034501.